SUPPLEMENTARY FIGURES

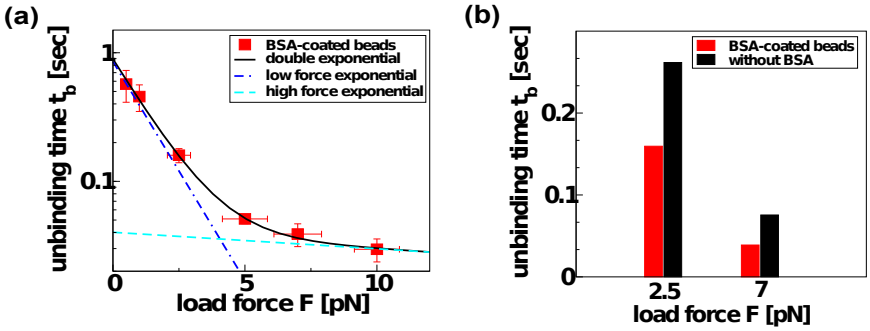

SUPPLEMENTARY FIGURE 1. Force dependence of the unbinding rate: (a) Force-dependence of the unbinding time (same data as in Fig. 2e) with single-exponential and double-exponential fits. (b) Effect of BSA-coating on the characteristic unbinding time at two different force values corresponding to the two different force regimes in (a) ($n > 35$ for each condition).

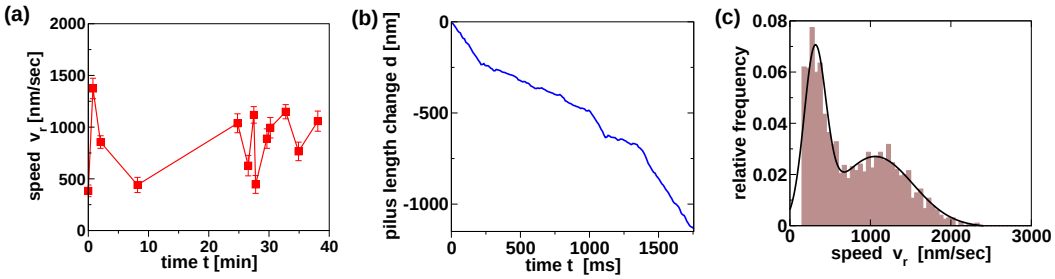

SUPPLEMENTARY FIGURE 2. Speed switching of pilus retraction at 120 pN. (a) Retraction speed v_r of consecutively measured single pilus retractions at 120 pN under aerobic conditions (average $\pm$ standard error, averaged over individual retraction events). (b) Frequent speed switching in a single pilus retraction event. (c) Bimodal speed distribution of all retraction events ($n = 41$). Solid line: Double-Gaussian fit.

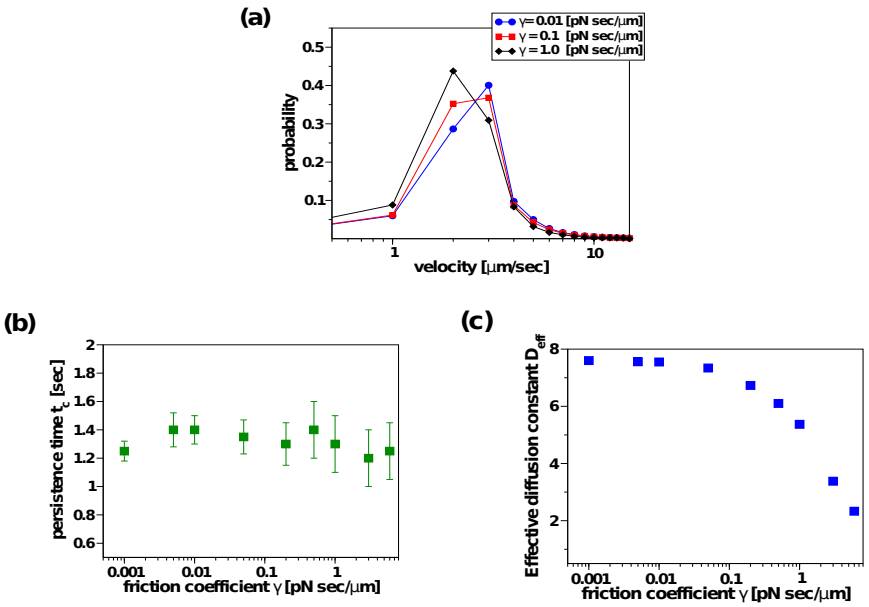

SUPPLEMENTARY FIGURE 3. Impact of the friction coefficient. (a) Velocity distribution for three different values of the friction coefficient γ. (b) Persistence time t_c (fitted parameter value $\pm$ standard error) and (c) effective diffusion coefficient D_{eff} as functions of the friction coefficient γ. The parameters are as in Supplementary Table 2 with $p_{\text{re}} = 0.2$ and $p_{\text{bld}} = 0.4$.

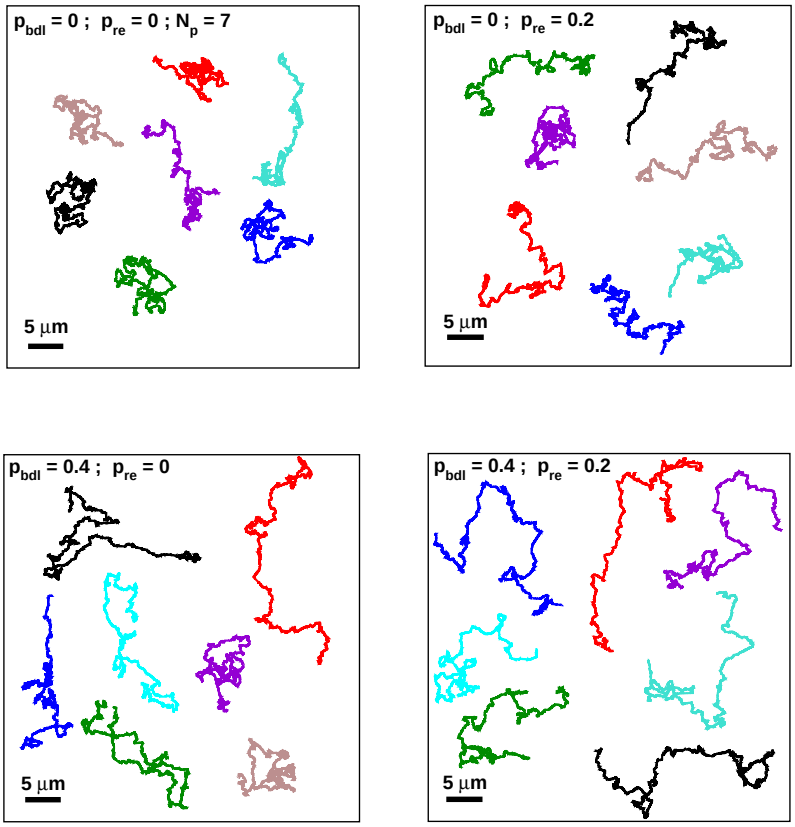

SUPPLEMENTARY FIGURE 4. Example trajectories from simulations with different bundling and re-elongation probabilities (p_{bdl} and p_{re}, respectively). All trajectories are 40 sec long, parameters are for wild type cells with, on average, $N_p = 7$ pili.

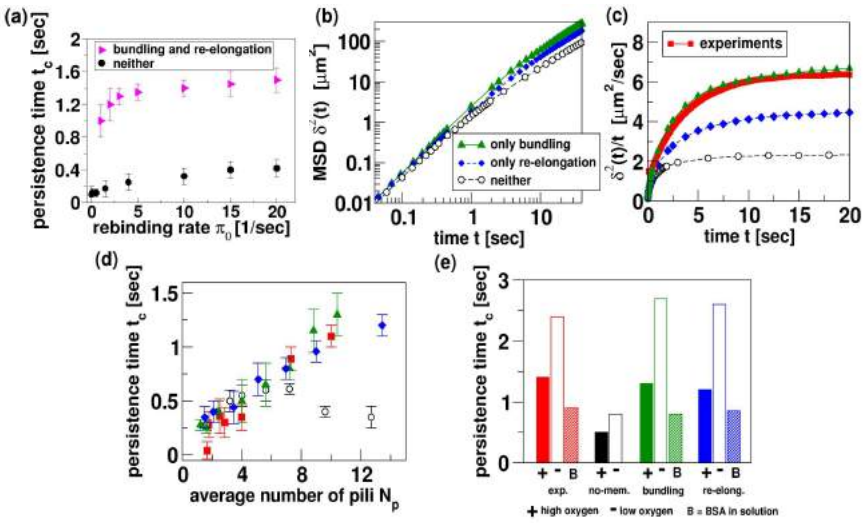

SUPPLEMENTARY FIGURE 5. Variation of parameters that have not been measured and memory requirement for persistent motion: (a) Variation of the rebinding rate π_0: Except for small π_0, the persistence time t_c (shown as fitted parameter value ± standard error in all panels) does not depend crucially on the rebinding rate. The parameters are those for WT bacteria (Supplementary Table 2, triangles); for the black circles, $p_{\rm bdl} = p_{\rm re} = 0$. (b-e) Variation of the bundling and re-elongation probabilities: Results corresponding to those of Fig. 5, but with either only bundling (green, $p_{\rm pdl} = 0.5$, $p_{\rm re} = 0$), only re-elongation (blue, $p_{\rm pdl} = 0$, $p_{\rm re} = 0.5$). These parameter sets lead to a persistence time consistent with the experimental value (Fig. 6a). The black curves show the case with neither bundling or re-elongation ($p_{\rm pdl} = p_{\rm re} = 0$), red data is from the motility experiments. (b) Mean square displacement $\delta^2(t)$ and (c) effective diffusion coefficient $\delta^2(t)/t$ as functions of time. Note that for the diffusion coefficient, the case with only bundling agrees better with the experimental data than the one with only re-elongation, although both have similar persistence times. (d) Persistence time as a function of pilus number for these three cases. For the bundling-only case (green), the bundling probability has been reduced ($p_{\rm bdl} = 0.4$) to mimic the effect of excess BSA present in these experiments (see Supplementary Note 4) and to match the experimental data (from ref. [1], red). In the case with re-elongation only, the data can also be matched by assuming a reduced re-elongation probability due to excess BSA ($p_{\rm re} = 0.4$, likewise for case B in panel (e)), there is however no experimental support for that assumption, so that bundling is required to explain the effect of excess BSA).

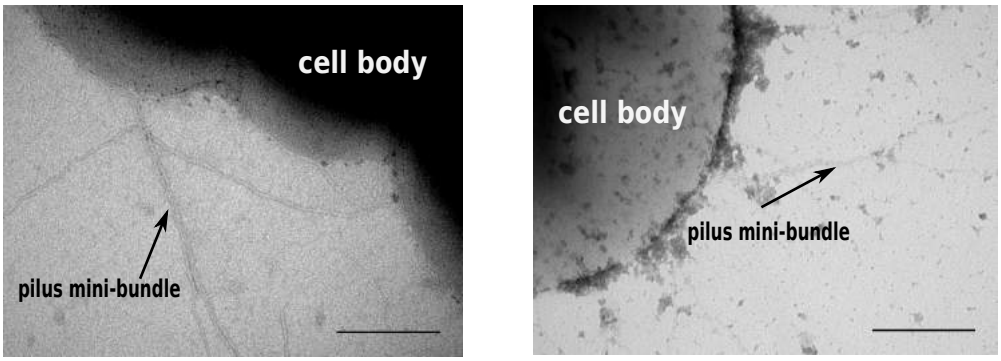

SUPPLEMENTARY FIGURE 6. Additional TEM images showing pilus mini-bundles (scale bar: 200 nm).

SUPPLEMENTARY TABLES

SUPPLEMENTARY TABLE I. Pilus length in the strain with inducible pilE

strain	number of cells	average number of pili per cell	pilus length* [μm]
$pilE_{ind}$, 0.05 mM IPTG	49	1.7	0.63 ± 0.36
$pilE_{ind}$, 0.25 mM IPTG	34	2.8	1.09 ± 0.17
N400 (WT)	82	7.3	0.80 ± 0.045

* parameter value ± standard error determined by an exponential fit to the distribution of pilus lengths

SUPPLEMENTARY TABLE II. Model parameters and values for wildtype bacteria as used in the simulations

Parameter	Symbol	Value	comments
pilus creation rate	c	9 sec^{-1}	chosen to adjust average pilus number N_p to 7 [1]*
rate of initial attachment	α_0	2.4 sec^{-1}	chosen to adjust average length of pili to 1μm [1]
rebinding rate	π_0	15 sec^{-1}	see text and Fig. 5a
unbinding rate	$\epsilon(F)$	force-dependent	$\epsilon(F) = [t_1 \exp(-\lvert F\rvert/F_{d,1}) + t_2 \exp(-\lvert F\rvert/F_{d,2})]^{-1}$
unbinding time scales	t_1	0.85 sec	see Fig. 2e
	t_2	0.04 sec	see Fig. 2e
unbinding forces	$F_{d,1}$	1.28 pN	see Fig. 2e
	$F_{d,2}$	33.8 pN	see Fig. 2e
retraction velocity	v_r	2 μm sec^{-1}	at zero force, see Fig. 2f, reduced to 1μm sec^{-1} under low-oxygen conditions
elongation velocity	v_e	2 μm sec^{-1}	similar to v_r [2]
stall force	F_s	180pN	see Fig. 2f
friction coefficient	γ	0.1 pN sec μm^{-1}	taken as comparable to Stokes friction (lower limit), see Supplementary Note 3
re-elongation probability	p_{re}	0.2	see text**
bundling probability	p_{bdl}	0.4	see text**, reduced to 0.2 in the presence of excess BSA
simulation time step	Δt	10^{-4} sec	

* $N_p \simeq 7$ for wild type. To describe the mutants with inducible *pilE* the number of pili is varied by varying c in the memory-less model and in the bundling model. The re-elongation probability is also modulated such that it is proportional to c.

** These parameters are varied in Fig. 6a and Supplementary Fig. 5. The values given here are used unless specified otherwise.

SUPPLEMENTARY TABLE III. Persistence times under different experimental conditions

condition	persistence time t_c [sec]*	
aerobic, with BSA-coated surface	1.4 ± 0.4	[1]
anaerobic, with BSA-coated surface	2.4 ± 0.7	this study
aerobic, with excess BSA in solution	0.9 ± 0.1	[1]

* fitted parameter value ± standard error.

SUPPLEMENTARY NOTES

Supplementary Note 1: Determination of unbinding times

We used a laser tweezers system with force feedback for measuring the distribution of unbinding times of pili from a BSA-coated glass surface. To this end, the bacterium was approached with a BSA-coated silica bead (Fig. 2a,b). When pilus retraction started, the bead was pulled out of the centre of the laser trap and thus the force increased steadily. At a preset force, the force-feedback was triggered by moving the sample with a piezo stage as to maintain the distance of the bead from the centre of the trap constant (Fig. 2c). The piezo movement is a measure for the length change of the pilus. The unbinding time t is defined as the time period between reaching the clamp force and the breaking of the pilus from the bead. Please note that the unbinding times are systematically underestimated due to the time it takes until the bead reaches the preset force. To minimise this effect, the stiffness of the trap was adjusted at different clamp forces. For each force, the distribution of unbinding times was exponential with a significant tail towards high unbinding times (Fig. 2d). As the data did not sufficiently specify this tail, we fitted a single exponential distribution and used the resulting characteristic unbinding time t_b for characterising the force-dependence of the unbinding process.

The dependence of the characteristic unbinding time on force was clearly inconsistent with a single exponential behaviour, but consistent with a double-exponential fit (Fig. 2e and Supplementary Fig. 1a). We also tested whether this behaviour depends on the BSA-coating of the beads. Without BSA coating, the unbinding times were longer both a low and high force (Supplementary Fig. 1b). The dependence of the unbinding time on the on the chemical nature of the surface (which we have seen qualitatively also from a comparison of glass and polystyrene beads in our previous work [1]) indicates that the observations indeed correspond to pilus unbinding rather than breaking of pili. Because the presence or absence of BSA influences the binding times at low and high force, we consider a simple interpretation of the double-exponential behaviour in which the two time scales correspond to unbinding from glass and from BSA, respectively, as unlikely. It is possible that multiple molecular bonds are responsible for pilus binding and that the number of molecular bonds may differ between the different retraction events. Thus the double-exponential behaviour may be

understood as a phenomenological description that serves as a basis for the theoretical description.

Supplementary Note 2: Global switching of type IV pili of *N. gonorrhoeae* between discrete states

Recently we showed, that the type IV pilus motor can switch between different states [3]. As long as oxygen is available the motor occupies a high speed mode. When oxygen is depleted the motor switches to the low speed mode. This behavior was detectable both by monitoring twitching motility and in optical tweezers experiments where motor switching on single pilus level in response to force was analyzed. The data for the persistence time of twitching under aerobic and anaerobic conditions are summarized in Supplementary Table 3. We note that the persistence times reported in [3] are higher than those reported in the present study. This difference is most likely due to slight variation between bacterial stocks and an improved evaluation of bacterial tracks. The method we use here is the same as in ref. [1].

At very high forces, switching between both states was observed even at high oxygen levels. At $F = 120$ pN, the average speed of subsequent retraction events showed a high variation (Supplementary Fig. 2a). When analysing the time course of individual retraction events, speed switching between a high speed mode and a low speed mode was sometimes observed (Supplementary Fig. 2b). The speed distribution of multiple pilus retractions at 120 pN clearly shows bimodal behavior (Supplementary Fig. 2c). This experiment demonstrates that speed switching can be triggered by the application of high force. Therefore, in Fig. 2f two different speed values are plotted at $F = 120$ pN. Since the pili most often detach from the surface before reaching such high forces, this effect was not taken into account in our models.

Supplementary Note 3: Estimation of the friction term

The force balance condition of our model (Equation 3 in the main text) contains a friction term that accounts for the drag of the bacterium in the fluid above the surface as well as for the interaction of the cell body with the surface. The value of the friction coefficient is not

known, but upper and lower limits can be estimated. The Stokes friction with the fluid leads to 0.1 pN sec/μm and can be considered as a lower limit. An upper limit can be estimated by considering that the velocity of the bacteria is only about 25% reduced compared to the retraction velocity of individual pili seen in the optical tweezers experiments (without movement of the cell body, thus representing low friction). Varying the friction coefficient in the model, we observe a reduction of the typical velocity values (as indicated by the peak at approximately 2 μm/sec in the velocity histograms in Supplementary Fig. 3a). Stronger reductions than seen experimentally are obtained if the friction coefficient exceeds the Stokes friction more than 10-fold (Supplementary Fig. 3a). Therefore we take the friction coefficient to be in the range between Stokes friction and this upper limit. The persistence time is rather insensitive to the value of the friction coefficient as shown in Supplementary Fig. 3b. The effective diffusion coefficient at long times, D_{eff} (Supplementary Fig. 3c) is dependent on the friction coefficient, but only varies by 20 percent in this range, reflecting the decreased velocity,

Supplementary Note 4: Excess BSA in solution in motility experiments

In experiments with the $pilE_{ind}$ strain and for one experimental condition in Fig. 5c, BSA for the coating of the glass surface was added to the medium [4] rather than coating and washing the surface as described above. Therefore, excess BSA was not washed away and was present in the medium in these experiments. Forces and velocities measured for single pili are the same in the presence of excess BSA in solution [4] and in its absence [5]. However, bundling of pili was reported to be reduced in the presence of BSA in the solution [6]. In agreement with that report, we found that the persistence time of twitching motility was reduced in the presence of BSA (ref. [1] and Supplementary Table 3), an effect that we can reproduce in our model by a reduced bundling probability (Fig. 5c). Solutions with excess BSA were also used for the experiments with the $pilE_{ind}$ strain. The rationale for this preparation was to increase the number of bacteria moving on the surface, which otherwise was very low for low levels of PilE. Under these conditions, the velocity and force generation

of single pili in the bacteria with fewer pili are not significantly different from wild type [4].

SUPPLEMENTARY REFERENCES

[1] Holz, C. *et al.* Multiple Pilus Motors Cooperate for Persistent Bacterial Movement in Two Dimensions. *Phys. Rev. Lett.* **104**, 178104 (2010).

[2] Skerker, J. M. & Berg, H. C. Direct observation of extension and retraction of type IV pili. *Proc. Natl. Acad. Sci. USA* **98**, 6901-6904 (2001).

[3] Kurre, R. & Maier, B. Oxygen Depletion and Speed Switching of a Bacterial Motor. *Biophys. J.* **102**, 2556-2563 (2012).

[4] Maier, B. *et al,* Single pilus motor force exceeds 100 pN. *Proc. Natl. Acad. Sci. USA* **99**, 16012-16017 (2002).

[5] Opitz, D., Clausen, M. & Maier, B. Dynamics of gonococcal type IV pili during infection. *Chem. Phys. Chem.* **10**, 1614-1618 (2009).

[6] Biais, N. *et al.* Cooperative Retraction of Bundled Type IV Pili Enables Nanonewton Force Generation. *PLoS Biol.* **6**, e87 (2008).